

Type of Non-reciprocity in Fiber Sagnac Interferometer induced by Geometric Phases

DONGZI ZHAO,¹ JING-ZHENG HUANG,¹ TAILONG XIAO,¹ HONGJING LI¹, XIAOYAN WU AND GUIHUA ZENG¹

¹State Key Laboratory of Advanced Optical Communication Systems and Networks, Institute of Quantum Sensing and Information Processing, Shanghai Jiao Tong University, Shanghai 200240, China

Abstract: The non-reciprocity of Sagnac interferometer provides ultra-high sensitivity for parameter estimation and offers a wide range of applications, especially for optical fiber sensing. In this work, we study a new type of non-reciprocity existed in optical fiber Sagnac interferometer where the polarization dependent loss is taken into consideration. In particular, this non-reciprocity is irrelevant to the physical effects that being considered in previous studies, which originates from the geometric phases induced by continuous-weak-measurement. In consequence, it has a unique phenomenon of sudden phase transition, which may open a new way for the future design of high precision optical fiber sensors.

© 2022 Optical Society of America under the terms of the [OSA Open Access Publishing Agreement](#)

1. Introduction

The optical fiber Sagnac interferometer plays important roles in various applications, such as fiber optic gyroscope (FOG) [1, 2], current detection [3], temperature sensing [4], strain detectors [5] and so on [6]. Standing in the heart of all these applications, it is the non-reciprocity of Sagnac loop induced by varying physical effects. However, the versatility of Sagnac interferometer sometimes becomes a curse for one to pursue high accuracy and precision. For example, in the case of FOG, the irrelevant effects caused by magnetic fields, thermal transits, acoustic fields and non-linearity of optic fiber [7, 8] will all induce undesired non-reciprocal phases, which dramatically limit the performance of the FOG and make constraints on the design of optic fiber coil to minimize these irrelevant effects [6].

In this work, a new type of non-reciprocity exists in fiber Sagnac interferometer is studied. Different from the previous studies, the non-reciprocal phase is irrelevant to the physical effects we mentioned above, but because the optical axes of the birefringence and polarization dependent loss (PDL) in the optic fiber are in different directions. Moreover, when the PDL strength reaches a certain level, there will be a sudden transition of this non-reciprocal phase. In the beginning, the phenomenon is proposed and analyzed based on the traditional transfer matrix method (TMM) [9, 10]. To further explore its origin, we employ a recent proposed continuous-weak-measurement model [11], and reveal its deep relation to the geometric phase.

This paper is organized as follows. The phenomenon of a new type non-reciprocity in Sagnac interferometer is presented along with a theoretical analysis based on TMM in Sec.II. Furthermore, the physical insight of this non-reciprocity is explored by using the model of continuous weak measurement and geometric phase in Sec.III, and the corresponding influences (both negative effects and potential for sensing) in the context of optical sensing are discussed Sec.IV. Finally, conclusions are made in Sec.V.

2. Principle

The basic idea of a fiber Sagnac interferometer is shown in Fig.1 [6]. The light ejected from a source passes through a beam splitter (Coupler 1) and a polarizer, and then divided into two beams by another beam splitter (Coupler 2), and then traverse along the clockwise (CW)

and counterclockwise (CCW) directions of the fiber ring respectively. Consequently, any time varying physical effects and inherently non-reciprocal phenomena can produce a non-reciprocal phase-shift, which can be finally detected by the detector placed on the other end of Coupler 1.

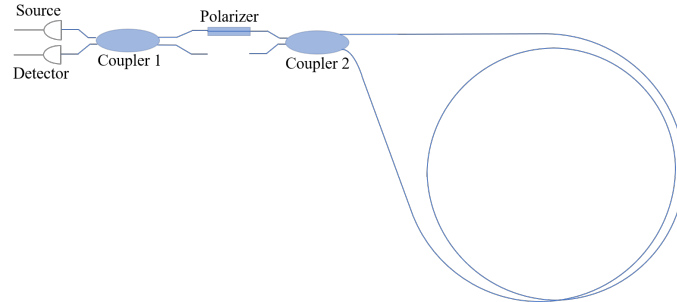


Fig. 1. The Schematic diagram of Sagnac interferometer.

As a common feature in optical fiber, the PDL can be easily generated by a number of physical effects. For examples, the pressure in the diametrical direction of the fiber will make the transmission coefficients of the two orthogonal polarization states being different, along with extra birefringence causing by the elasto-optic effect [12]. Similarly, the bending of the optical fiber will cause extra birefringence and extra PDL at the same time [13–18]. Although the PDL and the birefringence simultaneously appear in the fiber, their principal axes may in general be not coincident [19–22]. For simplicity, we assume the principal axes of the birefringence

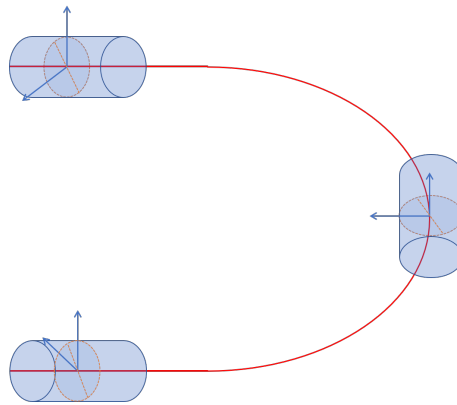


Fig. 2. A simple situation where the principal axes of PDL and birefringence in the fiber are differed by a fixed angle with respect to each other.

and PDL of the fiber loop in Fig.1 are fixed and differed by an angle θ_a with respect to each other, as is shown in Fig.2 and Fig.3. Here, we make the principal axes of birefringence as the laboratory coordinate. To analyze the evolution of optical polarization when the light traverses through the fiber loop, we divide the fiber loop into a series of small segments and employ the transfer matrix method (TMM) [10]. First, the optical fiber loop is divided into N segments, and the length (l) of each segment is made much smaller than the beat length of the optical fiber. We can then consider each of the segments as a combination of a birefringent wave plate and a non-ideal polarizer, as is depicted in Fig.4. The effective birefringent wave plate and non-ideal

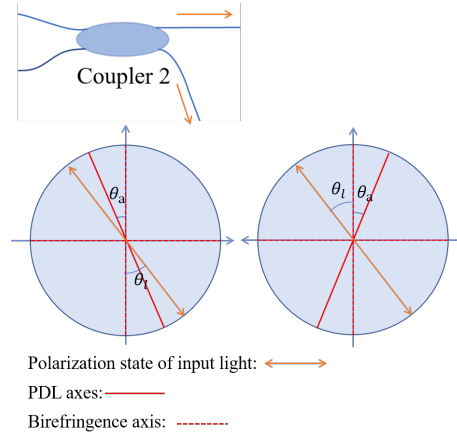


Fig. 3. Due to the geometric characteristics of the optical fiber loop, the principal axes of PDL and birefringence in the fiber exhibits ‘symmetric’ characteristics at the two ports. Here, θ_a represents the angle between the PDL axis and the birefringence axis, and θ_i represents the angle between linear input polarization and the birefringence axis.

polarized of the k th segment can be described by Jones matrices $\begin{bmatrix} 1 & 0 \\ 0 & e^{-i\phi_k} \end{bmatrix}$ and $\begin{bmatrix} 1 & 0 \\ 0 & \sqrt{\eta_k} \end{bmatrix}$ respectively, with the overall phase shift and transmittance being omitted for simplicity. Here, $\phi_k = 2\pi(n_o - n_e)l/\lambda$ is the phase difference introduced by the effective birefringent wave plate, with λ being the wavelength of the light, n_o and n_e being the refractive indexes along the two orthogonal principal axes. $\eta = T_{min}/T_{max} \approx 1$ is the PDL strength of the effective non-ideal polarizer, of which the polarization-dependent transmittance being denoted by T_{max} and T_{min} respectively. In consequence, the overall PDL strength of the optical fiber loop is given by

$$\Gamma_{dB} = -10 \log \eta^N = -10N \log \eta. \quad (1)$$

The Jones matrix of the k th segment can be expressed in the following form:

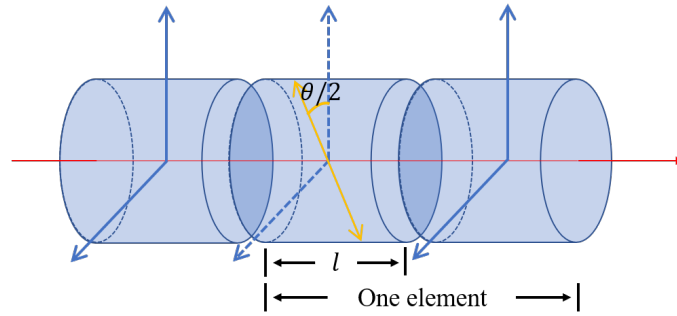


Fig. 4. A divided segment of the optical fiber.

$$\begin{bmatrix} \cos(\theta_k/2) & \sin(\theta_k/2) \\ \sin(-\theta_k/2) & \cos(\theta_k/2) \end{bmatrix} \begin{bmatrix} 1 & 0 \\ 0 & \sqrt{\eta_k} \end{bmatrix} \begin{bmatrix} \cos(\theta_k/2) & \sin(-\theta_k/2) \\ \sin(\theta_k/2) & \cos(\theta_k/2) \end{bmatrix} \begin{bmatrix} 1 & 0 \\ 0 & e^{-i\phi_k} \end{bmatrix}, \quad (2)$$

$$= R^{-1}(\theta_k)M_{\eta_k}R(\theta_k)C(\phi_k),$$

where $\theta_k/2$ is the angle between the principal axes of the effective non-ideal polarizer and effective phase plate.

We then consider an input light with linear polarization state of $|\psi_{in}\rangle = \begin{bmatrix} \cos(\theta/2) \\ \sin(\theta/2) \end{bmatrix}$. For simplicity, we assume that the axes and strengths of birefringence and PDL are time-invariant, which means $\theta_k = \theta$, $\eta_k = \eta$, $\phi_k = \phi$. Here we assume that PDL axis and input polarization are aligned, so the same $\theta/2$ is used to indicate the direction of the PDL axis and the input state. For the light propagating in the CW direction, the transfer matrix of the fiber loop evolves to be:

$$|\psi_{out+}\rangle = \prod R^{-1}(\theta)M_\eta R(\theta)C(\phi) |\psi_{in}\rangle. \quad (3)$$

On the other hand, the light propagating in the CCW direction evolves to be:

$$|\psi_{out-}\rangle = \prod C(\phi)R(\theta)M_\eta R^{-1}(\theta) |\psi_{in}\rangle. \quad (4)$$

By projecting both $|\psi_{out+}\rangle$ and $|\psi_{out-}\rangle$ back to the initial polarization state $|\psi_{in}\rangle$, the phase difference between the CW light and the CCW light can be obtained by:

$$\langle\psi_{out+}|\psi_{in}\rangle = \sqrt{I_+}e^{i\phi_+}, \langle\psi_{out-}|\psi_{in}\rangle = \sqrt{I_-}e^{i\phi_-}. \quad (5)$$

The change of phase difference $\phi_+ - \phi_-$ along with η by choosing specific values of θ is numerically simulated in Fig.5. Here we choose $N = 200$, $\psi = 2\pi/N$, the variation range of η is from 0.92 to 1, and the corresponding variation range of Γ_{dB} is from 84.56dB to 0dB. According to the numerical simulation results, we find that a phase transition appears when η reaches a certain value.

3. Theory

3.1. Theoretical analysis based on measurement-induced geometric phase

With assistance of TTM, we have discovered a new type of non-reciprocal phase induced by PDL, but its physical essence is not clear. In order to explain this phenomenon, we introduce a measurement-induced geometric phase theory that recently proposed by Gebhart, et al. [11]. In this theory, it was shown that Geometric phases are not necessarily a consequence of adiabatic time evolution, but can also be induced by a cyclic sequence of quantum measurements. Moreover, the mapping between the measurement sequence and the geometric phase undergoes a topological transition by varying the measurement strength [11]. The k th variable strength measurement can be written by the follow form:

$$M_k^{r_k}(\mathbf{n}_k, \eta_k) = \mathbf{R}^{-1}(\mathbf{n}_k)M_k^{r_k}(\mathbf{e}_z, \eta_k)\mathbf{R}(\mathbf{n}_k), \quad (6)$$

where $r_k \in \{+, -\}$ is the measurement readout, η_k is the measurement strength, and

$$M_k^+(\mathbf{e}_z, \eta_k) = \begin{bmatrix} 1 & 0 \\ 0 & \sqrt{\eta_k} \end{bmatrix}, M_k^-(\mathbf{e}_z, \eta_k) = \begin{bmatrix} 0 & 0 \\ 0 & \sqrt{1-\eta_k} \end{bmatrix} \quad (7)$$

are the operators of measurement on z direction, corresponding to the readouts of + and - respectively. And the operator

$$\mathbf{R}(\mathbf{n}_k) = \begin{bmatrix} \cos(\theta_k/2) & e^{-i\phi_k} \sin(\theta_k/2) \\ \sin(-\theta_k/2) & -e^{-i\phi_k} \cos(\theta_k/2) \end{bmatrix}, \quad (8)$$

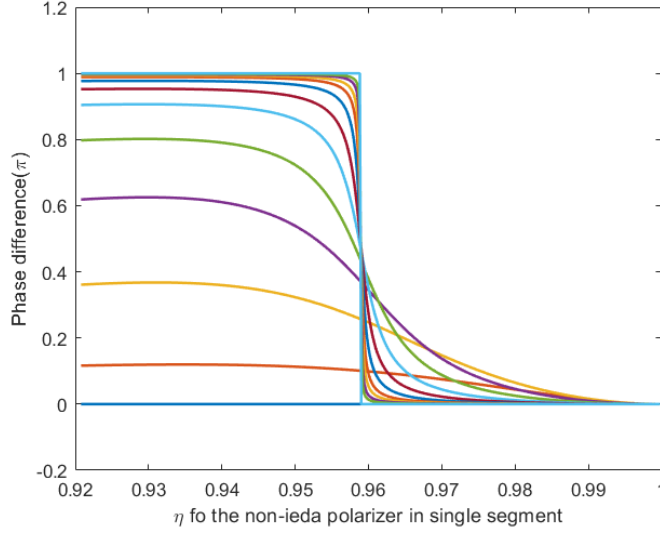


Fig. 5. Sorted by the left end of the curve, from bottom to top in the figure are the phase difference changes with η when $\theta = 0, \pi/4, 3\pi/8, 7\pi/16, 15\pi/32, 31\pi/64, 63\pi/128, 127\pi/256, 255\pi/512, 511\pi/1024, 1023\pi/2048, 2047\pi/4096, \pi/2$. It can be seen that as θ approaches $\pi/2$, the slope of the curve near $\eta = \eta_c$ will gradually increase until a sudden phase transition occurs, where $\eta_c \approx 0.96$. The variation range of η in the figure corresponds to the variation range of Γ_{dB} from 0dB to 84.56dB. At the transition point, $\Gamma_{dB} \approx 42dB$.

rotates the measurement orientation from z to $n_k = (\sin(\theta_k)\cos(\phi_k), \sin(\theta_k)\sin(\phi_k), \cos(\theta_k))$. Interestingly, the operator $M_k^+(\mathbf{n}_k, \eta_k)$ can be effectively implemented by rotating an imperfect polarizers and adding phase plate [11], which is perfectly matches the optical fiber segment model we have proposed in the last section. In particular, the PDL matrix M_η is exactly the same with $M_k^+(\mathbf{e}_z, \eta_k)$ if we consider the PDL strength as the measurement strength.

Therefore, the process described in Sec.II can be described a quasicontinuous measurement sequence with postselecting the results of $r_k = +$. According to the analysis made in Ref. [11], after N quasicontinuous measurements the initial state $|\psi_{in}\rangle$ becomes:

$$|\psi_N\rangle = M_N^+(\mathbf{n}_N, \eta_N)M_{N-1}^+(\mathbf{n}_{N-1}, \eta_{N-1})\dots M_1^+(\mathbf{n}_1, \eta_1)|\psi_{in}\rangle. \quad (9)$$

Different measurement sequences induce state trajectories on the Bloch sphere. For example, by taking $\theta_k = \pi/4$ and $\phi_k = 2\pi k/N$, the state trajectories under different measurement strength are depicted, as is shown in Fig.6. If $|\psi_N\rangle$ is then projected back to $|\psi_{in}\rangle$, the corresponding geometric phase induced by this process is $\chi_{geom} = \arg(\langle\psi_{in}|\psi_N\rangle)$. According to the geometric phase theory, this measurement-induced geometric phase can be equivalently expressed via the solid angle Ω of the trajectory on Bloch sphere by $\chi_{geom} = \Omega/2$ [23, 24].

Back to our analysis of the fiber Sagnac loop. Let us split the effective phase plate in the fiber segment by two parts (as is shown in Fig.6), and then $C(\phi_k)$ in Eq.(2) can be rewritten as

$$C(\phi_k) = \begin{bmatrix} 1 & 0 \\ 0 & e^{-i\phi_{k+1}} \end{bmatrix} \begin{bmatrix} 1 & 0 \\ 0 & e^{i\phi_k} \end{bmatrix} = C(\phi_{k+1})C^{-1}(\phi_k), \quad (10)$$

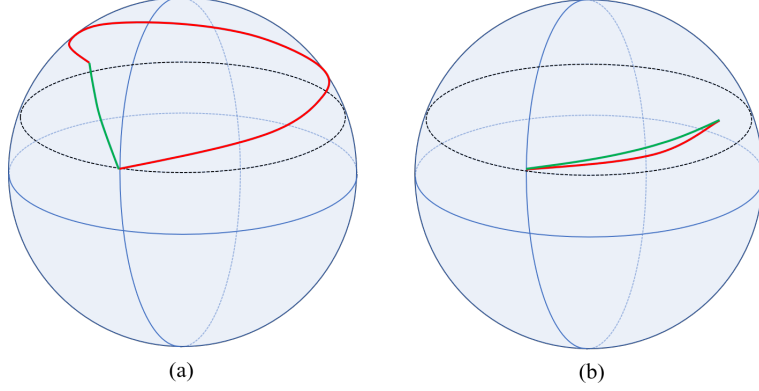


Fig. 6. When taking $\theta_k = \pi/4$ and $\phi_k = 2\pi/N$, the state trajectories under different measurement strength are depicted on the Bloch sphere. The circle drawn by the black dashed line represents the measurement orientation of the measurement sequences ($\{n_k\}$). The red curves in (a) and (b) represent the state trajectories under different measurement strength. And the green curves represent the final projection process. We can find that the solid angle of trajectory may be vary different under different measurement strength.

where $\phi_{k+1} - \phi_k = \phi$. Then Eq.(3) and Eq.(4) can be rewritten as:

$$\begin{aligned}
|\psi_{out}\rangle &= \dots C(\phi_{k+2})C^{-1}(\phi_{k+1})R^{-1}(\theta_{k+1})M_{\eta_{k+1}}R(\theta_{k+1})C(\phi_{k+1}) \\
&C^{-1}(\phi_k)R^{-1}(\theta_k)M_{\eta_k}R(\theta_k)C(\phi_k)C^{-1}(\phi_{k-1})\dots |\psi_{in}\rangle \\
&= \sum C^{-1}(\phi_k)R^{-1}(\theta_k)M_{\eta_k}R(\theta_k)C(\phi_k) |\psi_{in}\rangle.
\end{aligned} \tag{11}$$

Consequently, the transfer matrix connecting $|\phi_{k-1}\rangle$ and $|\phi_k\rangle$ is:

$$= \begin{bmatrix} \cos(\theta_k/2) & \sin(\theta_k/2) \\ e^{-i\phi_k} \sin(\theta_k/2) & -e^{-i\phi_k} \cos(\theta_k/2) \end{bmatrix} \begin{bmatrix} 1 & 0 \\ 0 & \sqrt{\eta_k} \end{bmatrix} \begin{bmatrix} \cos(\theta_k/2) & e^{-i\phi_k} \sin(\theta_k/2) \\ \sin(-\theta_k/2) & -e^{-i\phi_k} \cos(\theta_k/2) \end{bmatrix}, \tag{12}$$

which is coincident with Eq.(6). Consequently, the non-reciprocal phase difference between the light traverse along opposite directions in the fiber Sagnac loop can be interpreted as a PDL-induced geometric phase.

3.2. Numerical simulation

In order to study the PDL-induced non-reciprocity in the sense of geometric phase, we first recalculate the scenario that presented in Fig.5. By setting $\phi_k = 2k\pi/N$ ($k = 1, 2, 3 \dots N$), $\theta_k = \theta$ (with $0 < \theta < \pi$), $\eta_k = \eta$ (with $1 - \eta \ll 1$), and making the initial polarization state as $|\psi_{in}\rangle = \begin{bmatrix} \cos(\theta/2) \\ \sin(\theta/2) \end{bmatrix}$, we can plot the polarization state trajectory on the Bloch sphere that similar to the one shown in Fig.6.

Moreover, we find that the trajectory of polarization state on the Bloch sphere changes along with the PDL strength. Because the final projection will make the polarization state return to the initial state with the shortest trajectory on the Bloch sphere, as is shown in Fig.6.

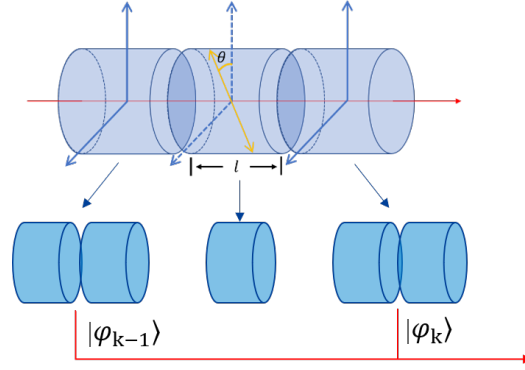


Fig. 7. Splitting the birefringent wave plate in each segment into two parts.

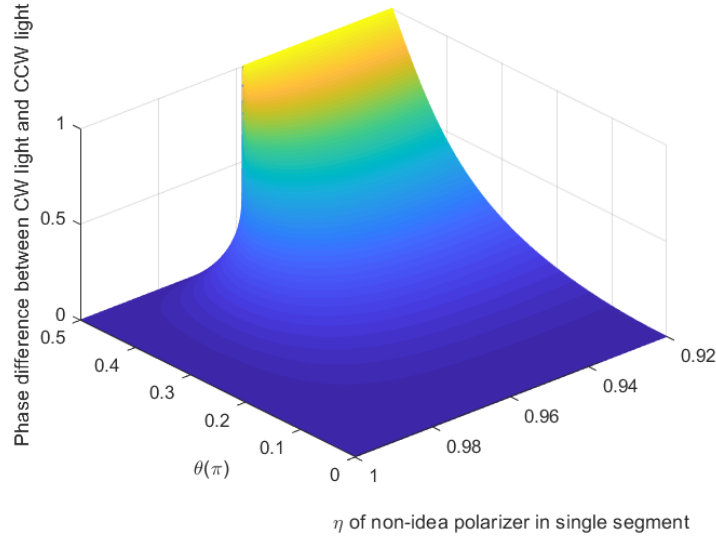


Fig. 8. The phase difference between CW light and CCW light varies with θ and η .

The PDL-induced non-reciprocal phases under different θ and η are calculated and depicted in Fig.8. In the case of weak PDL strength ($\eta > 0.96$), there is only a small fluctuation of the non-reciprocal phase with the change of θ , as is depicted in Fig.9 in red. In this case, the evolution trajectory of the polarization state (system state in the geometric phase theory) on the Bloch sphere is shown in Fig.6(a). We can find that the end point of the evolution trajectory cannot across the hemisphere. Therefore, after the final projection, the flux of the curved surface surrounded by the overall evolution trajectory yields a small value, corresponding to a small geometric phase. As the PDL strength increases, the end point of the evolution trajectory will finally crossed the hemisphere, and the solid angle of the trajectory will suddenly change, as shown in Fig.10(b). This happens at the point of $\eta = \eta_c \approx 0.96$ by setting $N = 200$. in our numerical simulation, and the sudden changed phase curve is depicted in Fig.9 in blue. After all, this phase transition can be explained by the sudden change of the solid angle of closed trajectory

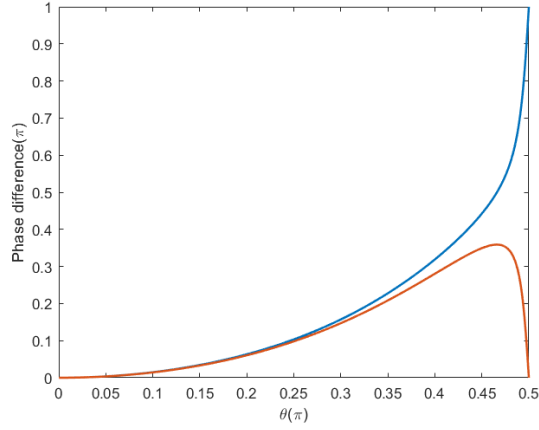


Fig. 9. The curve of the phase change with θ before(red) and after(blue) the phase transition point.

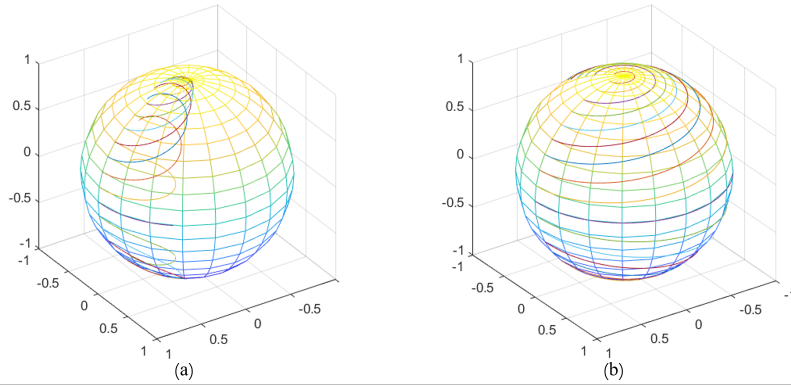


Fig. 10. The trajectory under different θ when $\eta > \eta_c$ (a) and $\eta < \eta_c$ (b).

on the Bloch sphere.

4. Discussions

4.1. Negative effects

In practice, the PDL in an optical fiber is usually weak, thus the non-reciprocal phase difference induced by PDL is also small. If the PDL-induced non-reciprocal phase is small comparing to the signal, this effect can be neglected. For instance, suppose the phase to be measured in the fiber Sagnac interferometer is in the order of $2\pi \times 10^{-2}$. If we consider that the PDL-induced non-reciprocal phase being an order of magnitude lower than the signal is tolerable, then the overall PDL of the fiber loop Γ_{dB} should be lower than 2.2dB. It is easily to be achieved in most of the optical fiber coils for normal applications.

However for a much smaller signal, the requirement for PDL strength will become more and more stringent. As is summarized in the following table, when the phase precision of the fiber Sagnac interferometer reaches to $2\pi \times 10^{-6}$, the effect of PDL-induced non-reciprocity can not be neglected if Γ_{dB} is larger than 0.0201dB. In this case, some parameters such as the radius of

the fiber coil should be carefully considered when designing the fiber Sagnac interferometer [20].

Phase precision	$2\pi \times 10^{-3}$	$2\pi \times 10^{-4}$	$2\pi \times 10^{-5}$	$2\pi \times 10^{-6}$
Maximum tolerable Γ_{dB}	0.8002dB	0.1603dB	0.0501dB	0.0201dB

Table 1. Maximum tolerable Γ_{dB} under different sensitivity requirements.

4.2. Potential for sensing

The sudden phase change happens at the phase transition point provides a good opportunity for high sensitivity parameter estimation. Specifically, we can make the new-type non-reciprocal phase very close to the phase transition point by introducing a high strength PDL. At this point, a very slight change on the PDL will cause an abrupt change on the phase, which indicates an ultrahigh sensitivity.

The extra PDL can be effectively introduced in many ways. For example, one can add an external pressure on a bent fiber from a different direction, as is shown in Fig.11. Here θ_s represents the angle between the directions of the pressure and the banding radius, but is not exactly equal to the one between the axes of extra birefringence and PDL, which requires more rigorous calculations [19–21]. According to the previous analysis and results shown in Fig.5, we would need a PDL strength of about 42dB, which can in principle be realized by a 210 turns of single mode fiber coil with a radius of 9mm, according to the results presented in Ref. [20]. This simple example is just for indicating the possibility. Many other possible ways, such as applying polarizing optical fiber or fiber Bragg grating, are worth to be explored for achieving the goal.

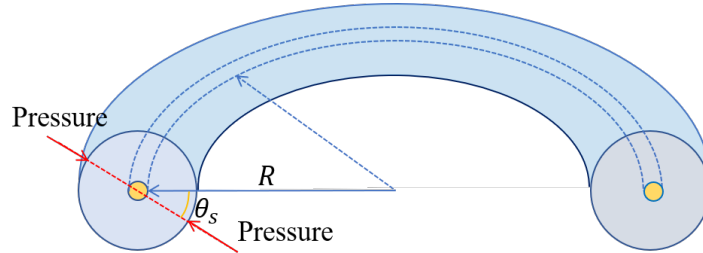


Fig. 11. Tilting the angle between the birefringence axis and the PDL axis by adding an external pressure on a bent fiber from a different direction. Here, R is the radius of curvature and θ_s is the angle between pressure direction and banding radius.

Moreover, in practice there are many other physical effects that can induce non-reciprocal phase in a fiber Sagnac loop, such as the power reflectance, Kerr effect, Faraday effect and so on, which will presented as noises in our sensing application. For example, the reflected power from the interfaces of devices may introduce so-called amplitude-type noise, and a broadband light source is required for suppressing this noise [25]. A more rigorous analysis on these kinds of noises and errors is an important issue in the future investigation.

5. Conclusion

In summary, we have found a new type of non-reciprocity in the optical fiber Sagnac interferometer, which is induced by the PDL (more precisely, the difference between the principal axes of PDL and birefringence). To explore the origin of this new non-reciprocity, we applied a recent proposed continuous-weak-measurement theory model and interpret the non-reciprocal phase as

a PDL-induced geometric phase. Fortunately, this effect is so small that it can be neglected for most of the common applications using fiber Sagnac interferometers, unless the requirement for precision is extremely high. Moreover, the numerical simulation indicates that a phase transition phenomenon will happen when the PDL strength reaches a certain value, which implies a new possibility for designing new type of sensors with ultra-high sensitivity.

Funding. This work was supported by the civil aerospace advance research project (D020403) and the National Natural Science Foundation of China (Grants No.62071298, No.61671287, No.61631014, and 193 No.61901258).

Disclosures. The authors declare that there are no conflicts of interest related to this article.

Data availability. Data underlying the results presented in this paper are not publicly available at this time but may be obtained from the authors upon reasonable request.

References

1. G. Sagnac. L'éther lumineux démontré par l'effet du vent relatif d'éther dans un interféromètre en rotation uniforme. (C. R. Acad. Sci. Paris, 1913) t.157, pp. 708–710.
2. D. H. Titterton, J. L. Weston. Strapdown Inertial Technology. (Amer Inst of Aeronautics, 1997).
3. J. Blake, P. Tantaswadi and R. T. de Carvalho, In-line Sagnac interferometer current sensor, IEEE Transactions on Power Delivery, vol. 11, no. 1, pp. 116-121, Jan. 1996, doi: 10.1109/61.484007.
4. L. Yundong, J. Xili, C. Hailiang, L. Jianshe, G. Ying, Z. Song, L. Hongyu, L. Shuguang. Highly sensitive temperature sensor based on sagnac interferometer using photonic crystal fiber with circular layout, Sensors and Actuators A: Physical, Volume 314, 2020, 112236, ISSN 0924-4247.
5. D. Xinyong, H. Y. Tam, P. Shum. Temperature-insensitive strain sensor with polarization-maintaining photonic crystal fiber based Sagnac interferometer, Appl. Phys. Lett. 90, 151113 (2007).
6. B. Culshaw. The optical fibre Sagnac interferometer: an overview of its principles and applications, 2005 Meas. Sci. Technol.
7. G. Agrawal. Nonlinear Fiber Optics. (New York: Academic, 2001) pp. 467.
8. Kurbatov, A.M., Kurbatov, R.A. Polarisation non-reciprocity cancelling in Sagnac fibre ring interferometer: an attempt of realistic study. Opt Quant Electron 51, 142 (2019).
9. J. Hao, L. Zhou, Electromagnetic wave scatterings by anisotropic metamaterials: Generalized 4×4 transfer-matrix method. Physical Review B, 2008, 77(9): 094201.
10. T. Xu, F. Tang, W. Jing, H. Zhang, D. Jia, X. Zhang, G. Zhou, Y. Zhang, Distributed measurement of mode coupling in birefringent fibers with random polarization modes, Optica Applicata, Vol. XXXIX, No. 1, 77- 90, 2009.
11. G. Valentin, S. Kyrylo, W. Thomas, B. Andreas, R. Alessandro, G. Yuval, Topological transition in measurement-induced geometric phases. PNAS March 17, 2020 117 (11) 5706-5713.
12. D. A. Jackson, R. Priest, A. Dandridge, and A. B. Tveten, Elimination of drift in a single-mode optical fiber interferometer using a piezoelectrically stretched coiled fiber, Appl. Opt. 19, 2926-2929 (1980)
13. S. C. Rashleigh and R. Ulrich, High birefringence in tension-coiled single-mode fibers, Opt. Lett. 5, 354-356 (1980)
14. A. M. Smith. Birefringence induced by bends and twists in single-mode optical fiber, Applied Optics, 1980, 19:2606-2611. D.
15. C. Vessallo, Optical Waveguide Concepts. (Elsevier, 1991).
16. Y. Zhou, W. Yu, H. Liu, J. Chen, P. Yang, L. She, C. Fang, J. Shao, Z. Guan, Z. Zhang, G. Feng, J. Yang, D. Chen. High-sensitive bending sensor based on a seven-core fiber. Optics Communications, Volume 483, 2021, 126617, ISSN 0030-4018.
17. D. Marcuse. (1977), Loss Analysis of Single-Mode Fiber Splices. Bell System Technical Journal, 56: 703-718.
18. D. Marcuse. Light Transmission Optics. New York, (Van Nostrand Reinhold Co, 1982).
19. Makoto Tsubokawa, Tsunehito Higashi, and Yukiyasu Negishi, Mode couplings due to external forces distributed along a polarization-maintaining fiber: an evaluation, Appl. Opt. 27, 166-173 (1988).
20. Q. Wang, G. Rajan, P. Wang, and G. Farrell, Polarization dependence of bend loss for a standard single mode fiber, Opt. Express 15, 4909-4920 (2007).
21. P. Wang, G. Farrell, Y. Semenova, Q. Wang, A. M. Hatta, and G. Rajan Accurate theoretical prediction for single-mode fiber macrobending loss and bending induced polarization dependent loss, Proc. SPIE 7003, Optical Sensors 2008, 70031Y (28 April 2008);
22. N. Brunner, A. Acín, D. Collins, N. Gisin, and Valerio, Scarani. Optical Telecom Networks as Weak Quantum Measurements with Postselection. Phys. Rev. Lett. 91, 180402(2003).
23. S. Pancharatnam. Generalized theory of interference and its applications. Proc. Indian Acad. Sci. 44, 398–417 (1956).
24. M. V. Berry. Quantal phase factors accompanying adiabatic changes. Proc. R. Soc, 1984, 392: 45-57.
25. H. Lefevre, The Fiber-Optic Gyroscope (2nd Ed.), (Artech House , 2014).